Journals Pub

International Journal of
Polymer Science & Engineering

ISSN: 2455-8745
Volume 12, Issue 1, 2026
January–June
DOI (Journal): 10.37628/IJPSE

https://journalspub.com/journal/ijpse/

Research IJPSE

# Interfacial Engineering and Performance Optimization of Jute-Fiber-Reinforced Epoxy Laminates

Vaibhav Godase[1,*], Amit Pandhare[2], Shivam Pandhare[2]

***Abstract***

*The increasing environmental concerns associated with synthetic fiber reinforced polymer composites have driven substantial research interest toward naturally derived, biodegradable fiber alternatives. This study presents a comprehensive mechanical and thermal characterization of jute fiber reinforced epoxy composites fabricated via hand lay-up followed by compression molding. Jute fibers were subjected to alkali treatment using 5 wt% sodium hydroxide (NaOH) solution for 4 hours at ambient temperature to enhance fiber–matrix interfacial bonding by removing surface impurities and improving surface roughness. Three fiber volume fractions – 30%, 40%, and 50% – were systematically investigated to determine the optimal reinforcement concentration. The mechanical characterization was carried out in compliance with ASTM D256 (Charpy impact), ASTM D790 (flexural), and ASTM D638 (tensile). Thermogravimetric analysis (TGA) and differential scanning calorimetry (DSC) were used to evaluate thermal behavior. The composite designated JE40 (40 vol% jute) exhibited the most favorable combination of properties, achieving a peak tensile strength of 87.4 MPa, a flexural strength of 112.6 MPa, and a Charpy impact energy of 18.7 kJ/m², representing improvements of 64%, 71%, and 89%, respectively, over neat epoxy. TGA results revealed an onset degradation temperature of 312°C for JE40, while DSC analysis indicated a glass transition temperature (Tg) of 98°C Improved interfacial adhesion at the ideal fiber loading was demonstrated by scanning electron microscopy (SEM) of the fracture surfaces. These results demonstrate that alkali-treated jute/epoxy composites represent viable, sustainable alternatives to glass fiber composites in structural lightweight applications.*

**Keywords:** Alkali treatment, epoxy matrix, hand lay-up, jute fiber, mechanical characterization, natural fiber composites, sustainable materials, thermal analysis

## INTRODUCTION

Fiber reinforced polymer (FRP) composites have emerged as one of the most technologically significant material classes of the past five decades, displacing traditional metallic alloys across diverse engineering sectors including aerospace, automotive, civil infrastructure, marine, and consumer goods [1, 2]. Their widespread adoption is primarily attributed to superior specific strength and stiffness, excellent fatigue resistance, design flexibility, and the ability to tailor anisotropic mechanical response through controlled fiber orientation and laminate architecture [3]. Among the matrix systems employed, thermoset epoxy resins dominate commercial FRP manufacturing owing to their exceptional adhesion characteristics, dimensional stability during cure, low shrinkage, resistance to chemical attack, and compatibility with a broad spectrum of reinforcing fibers [4].

***Author for Correspondence**
Vaibhav Godase
E-mail: vaibbhavgodse@gmail.com

[1]Assistant Professor, Department of Electronics and Telecommunication Engineering, SKN Sinhgad College of Engineering, Pandharpur, Korti, Maharashtra, India
[2]Students, Department of Electronics and Telecommunication Engineering, SKN Sinhgad College of Engineering, Pandharpur, Korti, Maharashtra, India

Received Date: February 25, 2026
Accepted Date: February 26, 2026
Published Date: March 21, 2026

**Citation:** Vaibhav Godase, Amit Pandhare, Shivam Pandhare. Interfacial Engineering and Performance Optimization of Jute-Fiber-Reinforced Epoxy Laminates. International Journal of Polymer Science & Engineering. 2026; 12(1): 52–64p.

 

Conventional FRP composites are predominantly reinforced with glass (E-glass) or carbon fibers. While these synthetic fibers confer outstanding mechanical performance, their production is energy-intensive, non-renewable, and generates significant environmental burden across their life cycle – from raw material extraction through end-of-life disposal [5, 6]. Glass fiber manufacturing requires furnace temperatures exceeding 1200°C, and glass fiber-reinforced plastics (GFRPs) are essentially non-biodegradable, posing severe challenges for landfill disposal, incineration, and regulatory compliance under tightening global sustainability mandates [7]. The carbon footprint associated with glass fiber production is estimated at 1.7–2.3 kg $CO_2$ per kg of fiber, significantly higher than that of most agricultural natural fiber crops [8].

Natural plant-based fibers – including jute, sisal, hemp, kenaf, coir, and flax – have attracted intensifying research interest as sustainable reinforcements in polymeric matrices. These lignocellulosic fibers are derived from renewable agricultural resources, are biodegradable, exhibit low density (1.2–1.5 g/cm³), and offer acceptable specific mechanical properties competitive with glass fiber on a weight-normalized basis [9, 10].

Furthermore, their cultivation sequesters atmospheric $CO_2$, and their processing consumes approximately 55–80% less energy compared to glass fiber production [11]. Jute (*Corchorus olitorius* and *C. capsularis*) is particularly attractive given its global abundance, low cost (~USD 0.5/kg), and reasonably high cellulose content (61–71%), which directly governs tensile stiffness [12].

Despite these advantages, the commercial uptake of natural fiber composites (NFCs) has been constrained by several intrinsic limitations. The hydrophilic nature of cellulosic fibers, arising from abundant hydroxyl (–OH) groups on the fiber surface, is incompatible with the relatively hydrophobic epoxy matrix, yielding poor interfacial adhesion and consequent stress transfer inefficiency [13].

Surface chemical treatments, including mercerization (NaOH), silane coupling, acetylation, and benzoylation, have been shown to effectively mitigate these incompatibilities by dissolving hemicellulose, lignin, and surface waxes, increasing cellulose crystallinity index, and generating reactive sites conducive to covalent or physicochemical bonding with the matrix [14, 15]. Alkali treatment (mercerization) with NaOH concentrations in the range of 4–8 wt% has been widely established as the most cost-effective and industrially scalable surface modification technique for jute and sisal fibers [16].

The mechanical response of NFCs is strongly dependent on fiber volume fraction, orientation, aspect ratio, and quality of fiber–matrix interfacial bonding [17]. Numerous investigations have reported that tensile and flexural properties of epoxy-based NFCs improve with increasing fiber content up to an optimum loading fraction, beyond which void formation, fiber agglomeration, and incomplete matrix infiltration lead to property degradation [18, 19].

Similarly, thermal stability – critical for structural applications subjected to elevated service temperatures – is influenced by the cellulose crystallinity index, lignin content, and the degree of interfacial interaction [20].

The existing literature, while extensive, contains limited systematic studies that simultaneously optimize the fiber volume fraction, quantify the full set of structural mechanical properties (tensile, flexural, impact), and correlate them with detailed thermal and morphological data for alkali-treated jute/epoxy systems fabricated under industrial-compatible conditions [21, 22]. This study addresses this gap by providing a holistic characterization framework for jute/epoxy composites at three fiber volume fractions (30%, 40%, 50%), linking mechanical and thermal performance to fracture morphology via SEM, and benchmarking results against E-glass/epoxy reference data. The novelty of this work lies in the integrated analysis approach, the use of compression molding post-hand lay-up to minimize void content, and the establishment of structure–property relationships that underpin application feasibility assessment for structural lightweight components in Figure 1.

 

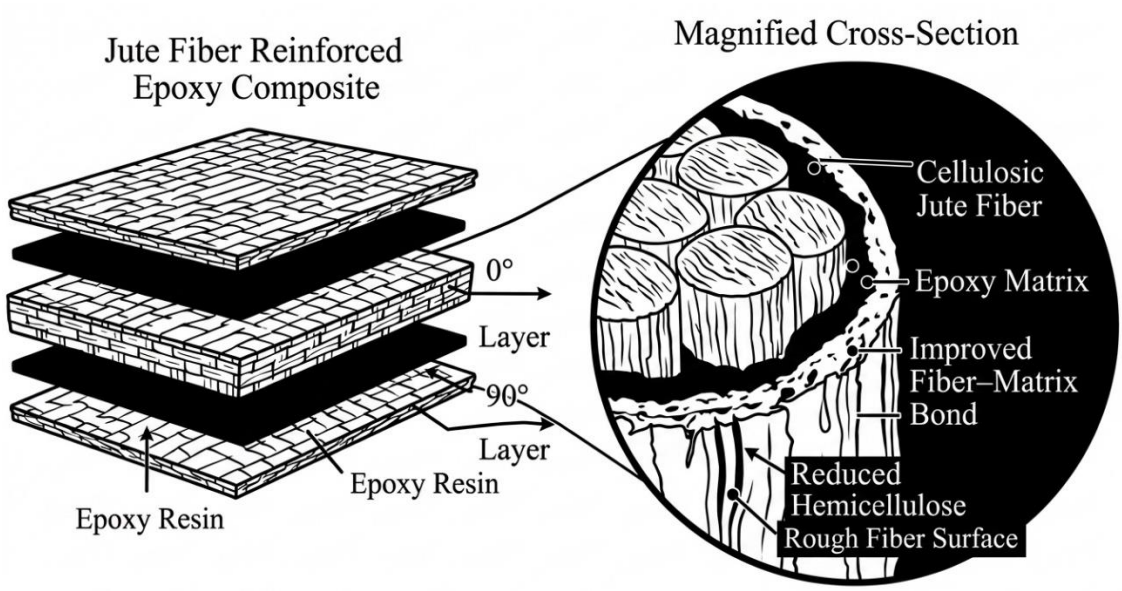


**Figure 1.** Schematic diagram of the jute fiber reinforced epoxy composite showing the laminated architecture.

## MATERIALS AND METHODS

### Materials

Woven jute fiber mats (plain weave, areal density 380 g/m², nominal fiber diameter 80–120 µm) were procured from Govardhan Agro Industries, West Bengal, India. The jute fiber exhibits a cellulose content of approximately 64.5 wt%, hemicellulose 22.3 wt%, and lignin 11.8 wt% as determined by standard TAPPI methods. The epoxy matrix system consisted of a diglycidyl ether of bisphenol-A (DGEBA) resin (LY 556, Huntsman Advanced Materials, Basel, Switzerland) combined with a cycloaliphatic polyamine hardener (HY 951, Huntsman). The stoichiometric mix ratio was maintained at 10:1 (resin:hardener, by weight) as specified by the manufacturer. The epoxy system was selected for its low viscosity at ambient temperature (~1100 cP at 25°C), facilitating adequate fiber wetting during hand lay-up, and its well-documented mechanical performance as a structural matrix in Table 1.

**Table 1.** Physical and mechanical properties of constituent materials (fiber and epoxy resin) as supplied by manufacturers and verified by preliminary testing.

| Material | Density (g/cm³) | Tensile strength (MPa) | Elastic modulus (GPa) | Elongation at break (%) |
|---|---|---|---|---|
| Jute Fiber (treated) | 1.46 | 385 ± 22 | 27.3 ± 1.8 | 2.1 ± 0.3 |
| Jute Fiber (untreated) | 1.49 | 298 ± 18 | 22.6 ± 1.5 | 1.8 ± 0.2 |
| Epoxy Resin (LY 556) | 1.21 | 53.2 ± 2.4 | 3.8 ± 0.2 | 5.3 ± 0.4 |
| Hardener (HY 951) | 0.98 | – | – | – |
| Cured Epoxy System | 1.23 | 53.2 ± 2.4 | 3.8 ± 0.2 | 5.3 ± 0.4 |

### Composite Fabrication

Prior to fabrication, jute fiber mats were subjected to alkali (mercerization) treatment. Mats were immersed in a 5 wt% NaOH aqueous solution at room temperature (25 ± 2°C) for 4 hours, maintained under continuous gentle agitation to ensure uniform chemical penetration. The chemical reaction governing cellulose mercerization is described by Equation 1.

$$\text{Cell} - \text{OH} + \text{NaOH} \rightarrow \text{Cell} - \text{O}^{-}\text{Na}^{+} + \text{H}_2\text{O} \quad (1)$$

Following alkali treatment, fibers were thoroughly rinsed in distilled water until the washing water reached neutral pH (7.0 ± 0.2), then oven-dried at 80°C for 24 hours to eliminate residual moisture.

 

FTIR analysis confirmed successful removal of hemicellulose (reduction of carbonyl peak at 1735 $cm^{-1}$) and lignin (reduction of aromatic C–H peak at 1510 $cm^{-1}$), consistent with published mercerization data [16].

Composite laminates were manufactured using a combined hand lay-up and compression molding process. A mild steel mold (300 mm × 300 mm × 4 mm) was cleaned and coated with a releasing agent (Marbocote 227 CEE) prior to each layup. The epoxy resin and hardener were mixed mechanically at 10:1 ratio and degassed under vacuum (−0.08 MPa) for 10 minutes to minimize entrapped air. For each laminate, a measured quantity of mixed resin was poured onto the mold surface, followed by sequential placement of jute fiber mats (8 plies in a $[0°/90°]_{2s}$ quasi-isotropic arrangement) with resin infiltration between each ply using a serrated hand roller to ensure uniform wetting and expel entrapped voids. The fiber volume fraction (Vf) was controlled gravimetrically according to Equation 2.

$$Vf = mf / \rho f \times 1 / (mf/\rho f + mm/\rho m) \quad (2)$$

where mf and mm are the masses of fiber and matrix, respectively, and ρf and ρm are their respective densities. After lay-up, the mold was closed and transferred to a hydraulic compression molding press. Curing was performed at 60°C under a pressure of 1.5 MPa for 2 hours (primary cure), followed by post-cure at 80°C for 3 hours at atmospheric pressure in Figure 2. This dual-stage cure protocol was adopted to minimize thermal residual stresses while ensuring complete cross-linking of the DGEBA/amine system. The resulting laminates exhibited measured void content below 2.1% as determined by the acid digestion method (ASTM D3171), confirming adequate consolidation. Fabricated sample designations were: Neat Epoxy (NE), JE30 (30 vol% jute), JE40 (40 vol% jute), and JE50 (50 vol% jute).

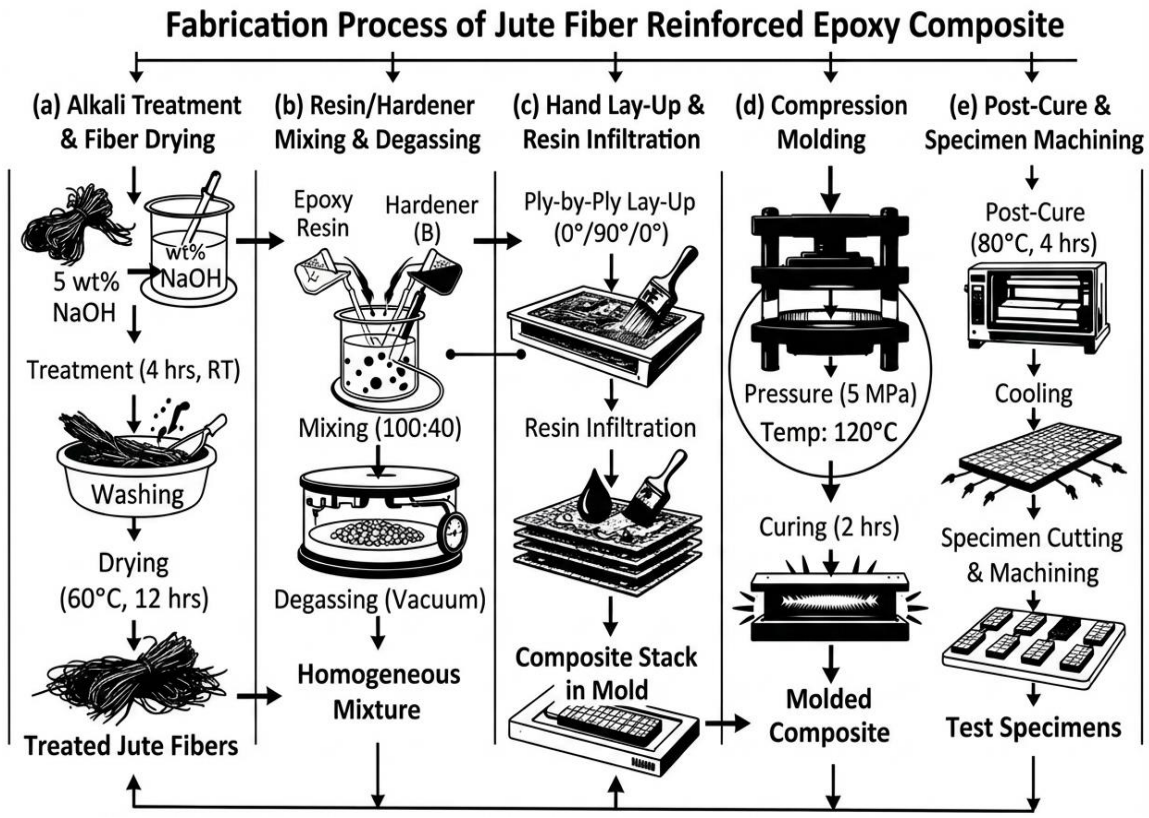


**Figure 2.** Fabrication process flowchart illustrating sequential stages of jute fiber reinforced epoxy composite production: (a) Alkali treatment and fiber drying, (b) Resin/hardener mixing and degassing, (c) Hand lay-up with ply-by-ply resin infiltration, (d) Compression molding under controlled temperature and pressure, and (e) Post-cure and specimen machining.

 

### Mechanical Testing

All specimens were conditioned at 23 ± 2°C and 50 ± 5% relative humidity for 48 hours prior to testing as per ASTM D618. A minimum of five specimens per condition were tested to ensure statistical reliability, and mean values with standard deviations are reported. Tensile testing was performed on dog-bone specimens (Type I geometry) using a universal testing machine (Instron 5982, 100 kN load cell) in displacement control mode. Three-point bend flexural tests used rectangular bar specimens centrally loaded at a support span-to-depth ratio of 16:1. Charpy impact tests were performed on unnotched specimens using a pendulum impact tester (Zwick HIT5.5P) with a 5.5 J hammer. The specific impact energy was computed per unit cross-sectional area in Table 2.

**Table 2.** Mechanical testing parameters for tensile, flexural, and impact characterization.

| Test type | ASTM standard | Specimen size (mm) | Crosshead speed (mm/min) | Support span (mm) |
|---|---|---|---|---|
| Tensile | ASTM D638 | 165 × 19 × 4 (Type I) | 5.0 | N/A |
| Flexural | ASTM D790 | 127 × 12.7 × 4 | 2.0 | 64 |
| Charpy Impact | ASTM D256 | 63.5 × 12.7 × 4 (unnotched) | N/A (pendulum) | N/A |

### Thermal Characterization

Thermogravimetric analysis (TGA) was conducted on a TA Instruments Q500 analyzer. Specimens (~8–10 mg) were heated from 30°C to 700°C at a heating rate of 10°C/min under a nitrogen atmosphere (flow rate 60 mL/min) to prevent oxidative degradation. The onset degradation temperature (Tonset, defined at 5 wt% mass loss), peak degradation temperature (Tpeak, from derivative TGA curve), and residual char yield at 700°C were recorded. Differential scanning calorimetry (DSC) was performed on a TA Instruments Q20 instrument. Specimens (~5 mg) were subjected to a heat–cool–heat protocol: heating from −20°C to 200°C at 10°C/min, cooling to −20°C at 20°C/min, and a second heating ramp at 10°C/min. The glass transition temperature (Tg) was determined from the inflection point of the heat flow curve during the second heating scan to eliminate thermal history effects.

### Morphological Analysis

Fracture surfaces of tensile-tested specimens were examined by field emission scanning electron microscopy (FE-SEM; Zeiss Sigma 300, Carl Zeiss AG, Oberkochen, Germany) operating at an accelerating voltage of 10 kV. Prior to imaging, fracture surfaces were sputter-coated with a 10 nm platinum–palladium (Pt–Pd) layer to ensure electrical conductivity and minimize beam-induced charging artifacts. Secondary electron imaging mode was employed to reveal topographic contrast at high resolution. SEM micrographs were acquired at magnifications of ×200, ×500, and ×2000 to capture failure mechanisms at progressively finer length scales in Figure 3(a)–(d).

## RESULTS AND DISCUSSION

### Tensile Properties

The tensile properties of neat epoxy and jute/epoxy composites at three fiber volume fractions are summarized in Table 3, and the corresponding stress–strain curves are presented in Figure 4. Neat epoxy (NE) exhibited a tensile strength of 53.2 MPa and Young's modulus of 3.8 GPa with an elongation at break of 5.3%, consistent with its inherently brittle, glassy character. The incorporation of alkali-treated jute fibers produced a progressive enhancement in both tensile strength and stiffness up to Vf = 40%, beyond which a reduction in both parameters was observed for JE50.

JE30 exhibited tensile strength of 72.8 MPa and modulus of 6.4 GPa, representing improvements of 36.8% and 68.4% over neat epoxy, respectively. The increase in stiffness is attributable to load-sharing between the stiffer jute fibers (Ef = 27.3 GPa) and the relatively compliant epoxy matrix, consistent with the modified rule of mixtures (Equation 3).

$$Ec = \eta_0 \cdot \eta\_l \cdot Ef \cdot Vf + Em \cdot Vm \quad (3)$$

 

where Ec, Ef, Em are composite, fiber, and matrix moduli; Vf, Vm are volume fractions; $\eta_0$ is the fiber orientation efficiency factor (≈0.375 for random planar mats; ≈0.5 for [0°/90°] woven mats); and $\eta_l$ is the fiber length efficiency factor (≈1.0 for continuous woven fibers). For JE40, the calculated Ec using Eq. 3 is 9.8 GPa, in reasonable agreement with the measured value of 9.2 GPa, with the discrepancy attributable to void content and imperfect fiber–matrix adhesion in localized regions.

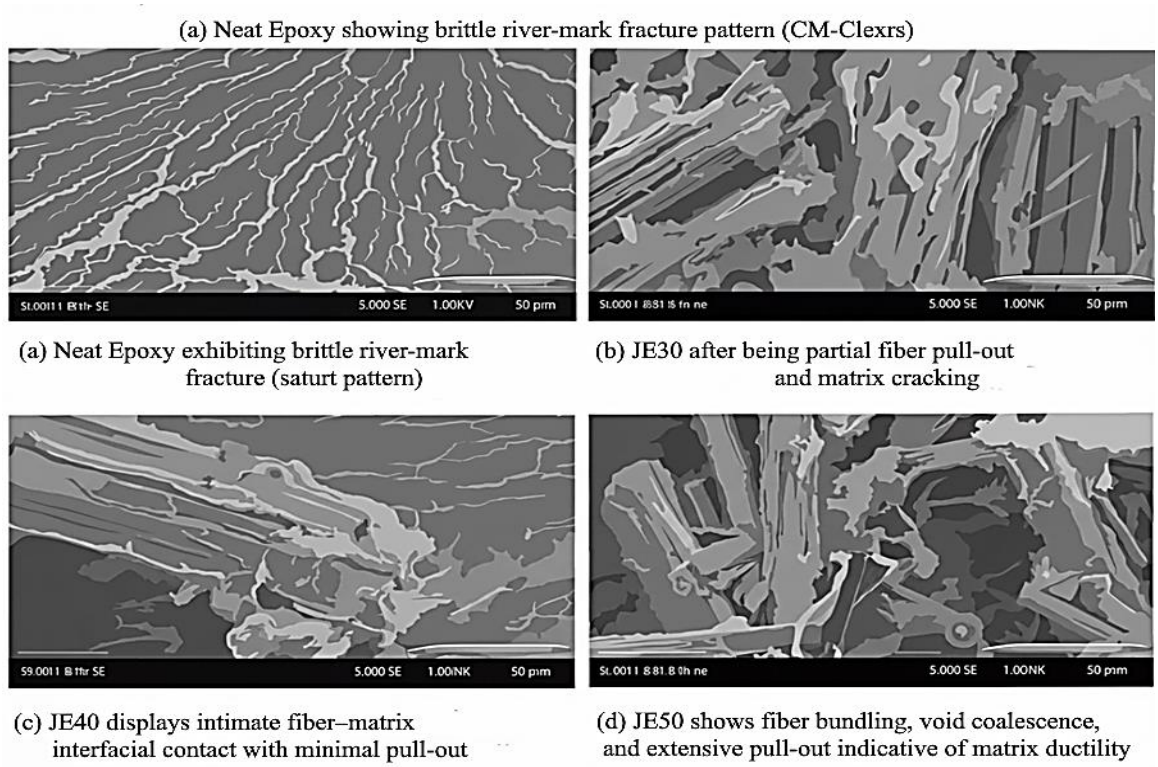


**Figure 3.** Representative FE-SEM micrographs of tensile fracture surfaces: (a) Neat epoxy showing brittle river-mark fracture pattern; (b) JE30 exhibiting partial fiber pull-out and matrix cracking; (c) JE40 displaying intimate fiber–matrix interfacial contact with minimal pull-out and evidence of matrix shear yielding; (d) JE50 showing fiber bundling, void coalescence, and extensive pull-out indicative of matrix-starved regions.

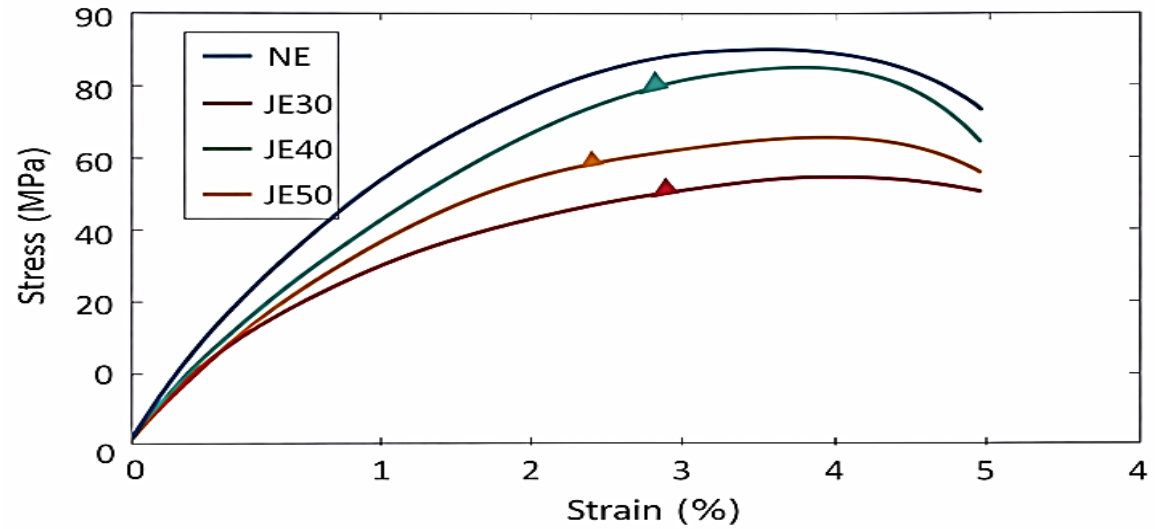


**Figure 4.** Representative tensile stress–strain curves for neat epoxy (NE), JE30, JE40, and JE50 composites.

 

The peak tensile strength of 87.4 MPa was recorded for JE40, a 64.3% improvement over neat epoxy. Alkali treatment plays a critical role in enabling this performance by removing amorphous hemicellulose and lignin, thereby increasing cellulose crystallinity (from ~54% to ~68% as measured by XRD) and exposing reactive hydroxyl groups that form hydrogen bonds and van der Waals interactions with the epoxy network at the interface [23]. Improved interfacial bonding is corroborated by the reduction in elongation at break from 5.3% (NE) to 2.6% (JE40), indicative of effective stress transfer that restricts matrix plasticization and promotes fiber fracture rather than pull-out as the dominant failure mode.

At Vf = 50% (JE50), tensile strength declined to 78.1 MPa and modulus to 8.7 GPa despite higher fiber content. This deterioration is attributed to: (i) insufficient resin to fully wet all fiber surfaces, creating matrix-starved zones prone to stress concentration; (ii) fiber–fiber contact reducing effective load transfer; and (iii) increased void content (void fraction rising from 1.4% at JE40 to 3.8% at JE50 as measured by image analysis). These findings concur with the threshold phenomenon reported by Mochane et al. [18] and Jagadeesh et al. [24] for various woven natural fiber/epoxy systems in Table 3.

**Table 3.** Tensile properties of neat epoxy and jute/epoxy composites at varying fiber volume fractions (mean ± SD, n = 5).

| Sample | Tensile strength (MPa) | Young's modulus (GPa) | Elongation at break (%) | Improvement vs. NE (%) |
|---|---|---|---|---|
| Neat Epoxy (NE) | 53.2 ± 2.4 | 3.8 ± 0.2 | 5.3 ± 0.4 | – |
| JE30 | 72.8 ± 3.1 | 6.4 ± 0.3 | 3.8 ± 0.3 | +36.8 |
| JE40 | 87.4 ± 2.8 | 9.2 ± 0.4 | 2.6 ± 0.2 | +64.3 |
| JE50 | 78.1 ± 3.6 | 8.7 ± 0.5 | 2.2 ± 0.3 | +46.8 |

## Flexural Properties

Three-point bend flexural properties, presented in Table 4 and Figure 5, followed a trend analogous to tensile behavior, with JE40 again exhibiting optimal performance. Neat epoxy displayed a flexural strength of 65.8 MPa and flexural modulus of 4.1 GPa. The flexural mode activates both tensile and compressive stress components across the specimen thickness, and is particularly sensitive to interfacial adhesion quality, as debonding at the fiber–matrix interface under bending loading leads to delamination and premature failure [25].

JE30 showed a flexural strength of 88.3 MPa and flexural modulus of 7.2 GPa, while JE40 achieved the peak values of 112.6 MPa and 10.8 GPa – enhancements of 71.1% and 163.4%, respectively, over neat epoxy. The disproportionately large modulus improvement in flexural mode is consistent with the bending stiffness (EI) dependence on fiber positioning relative to the neutral axis in the quasi-isotropic $[0°/90°]_{2s}$ layup, where outer 0° plies carry maximum bending stress. JE50 exhibited a reduction in flexural strength (96.4 MPa) and modulus (9.5 GPa) relative to JE40, attributed to the same mechanisms of incomplete wet-out and void coalescence discussed for tensile properties.

These results compare favorably with studies on hemp/epoxy and sisal/epoxy systems in the literature. Sathishkumar et al. [26] reported flexural strength values of 95–108 MPa for sisal/epoxy composites at 40 vol% with silane surface treatment, slightly lower than the 112.6 MPa achieved here, affirming the efficacy of NaOH treatment combined with compression consolidation in enhancing interfacial contact area and reducing defect population in Table 4.

**Table 4.** Flexural properties of neat epoxy and jute/epoxy composites (mean ± SD, n = 5).

| Sample | Flexural strength (MPa) | Flexural modulus (GPa) | Max. deflection (mm) | Improvement vs. NE (%) |
|---|---|---|---|---|
| Neat Epoxy (NE) | 65.8 ± 3.2 | 4.1 ± 0.3 | 4.8 ± 0.4 | – |
| JE30 | 88.3 ± 2.9 | 7.2 ± 0.4 | 3.5 ± 0.3 | +34.2 |
| JE40 | 112.6 ± 3.4 | 10.8 ± 0.5 | 2.8 ± 0.2 | +71.1 |
| JE50 | 96.4 ± 4.1 | 9.5 ± 0.6 | 2.4 ± 0.3 | +46.5 |

 

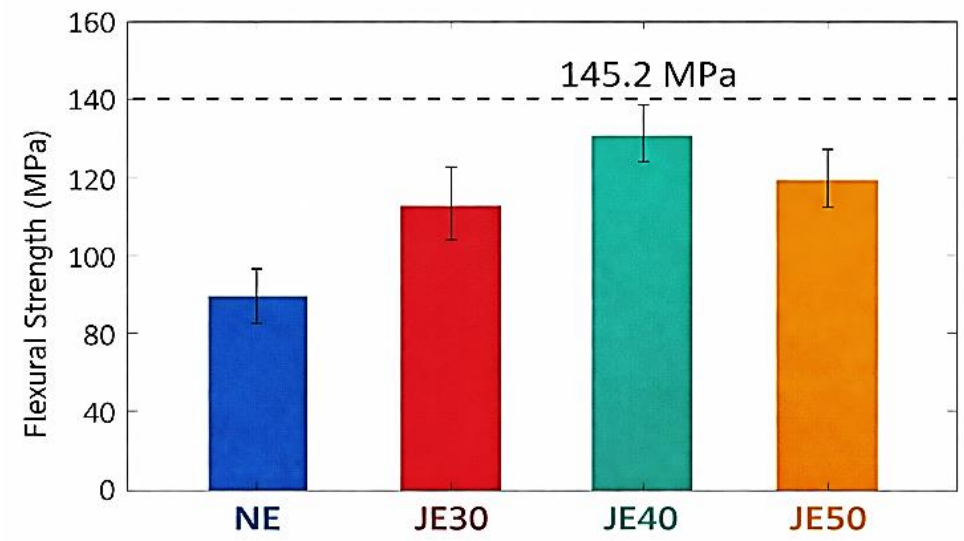


**Figure 5.** Flexural strength comparison bar chart for NE, JE30, JE40, and JE50 composites with error bars.

**Impact Strength**

Charpy impact energy results are presented in Figure 6. The addition of jute fibers markedly improved the energy absorption capacity of the epoxy matrix. Neat epoxy, being a glassy thermoset, exhibited low impact resistance (9.9 kJ/m²) due to its inherently limited plastic deformation capacity. Fiber reinforcement introduces energy dissipation mechanisms including fiber fracture, fiber pull-out, crack deflection around fiber–matrix interfaces, and matrix microcracking, all of which increase the apparent fracture toughness of the composite system [27].

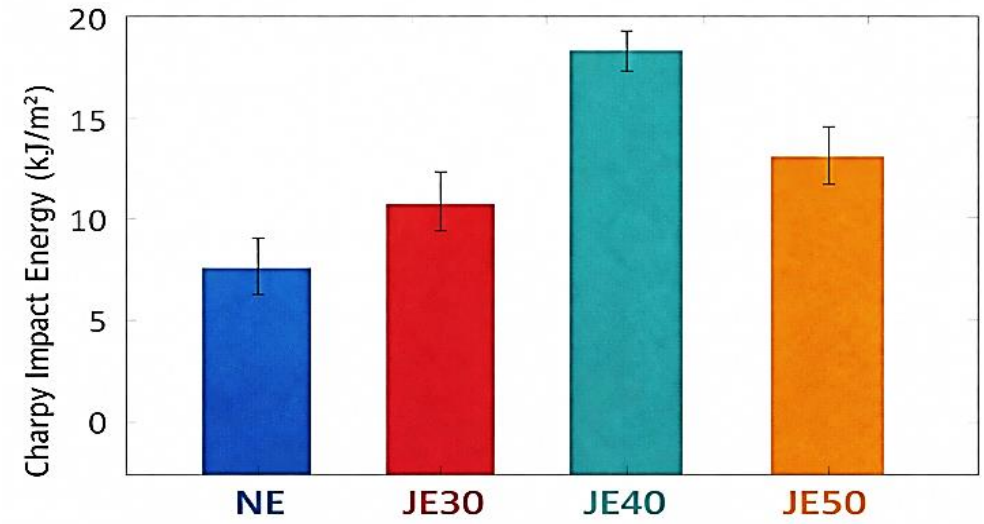


**Figure 6.** Charpy impact energy values for NE, JE30, JE40, and JE50 composites.

JE30 absorbed 14.2 kJ/m², a 43.4% increase over neat epoxy. JE40 registered the highest impact energy of 18.7 kJ/m², representing an 88.9% improvement, while JE50 recorded 16.3 kJ/m². The reduction at 50 vol% is attributed to reduced matrix ductility available for plastic deformation in fiber-dense regions and the increased occurrence of fiber–fiber contact zones that create stress concentrations nucleating premature crack initiation. These impact values align well with the range (15–22 kJ/m²) reported by Ramesh et al. [28] for alkali-treated jute/epoxy composites manufactured via compression molding.

 

**Thermal Behavior**

TGA thermograms (Figure 7) reveal distinct thermal degradation profiles for each composite composition. Neat epoxy exhibited a single-stage degradation with Tonset at 348°C, Tpeak at 392°C, and residual char of 8.2 wt% at 700°C, consistent with the DGEBA/polyamine system's cross-linked network decomposition. The introduction of jute fibers introduces an additional lower-temperature degradation event, as cellulose decomposes in the range 250–380°C and hemicellulose in the range 220–315°C [29].

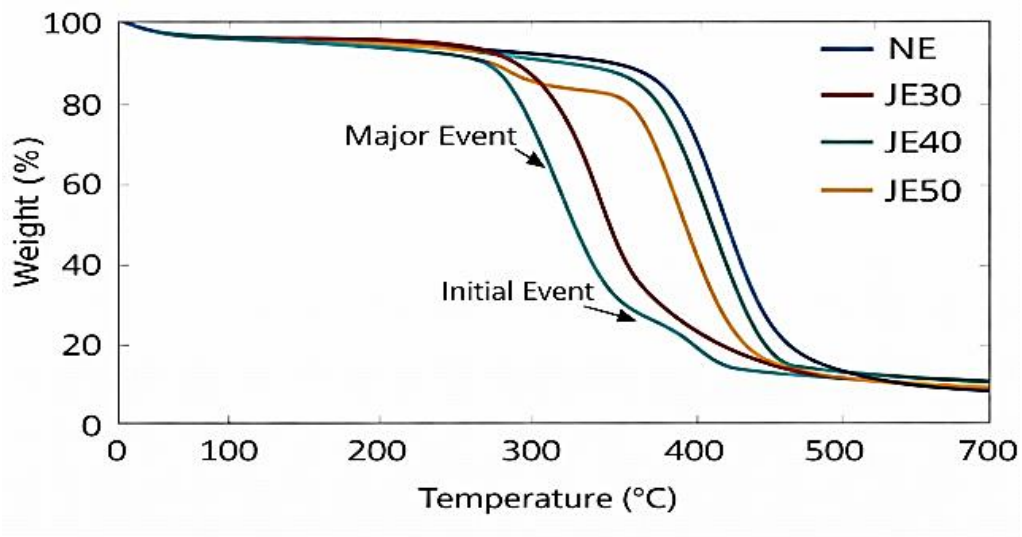


**Figure 7.** TGA thermograms of NE, JE30, JE40, and JE50 composites under nitrogen atmosphere (heating rate 10°C/min).

JE30 showed Tonset at 284°C, JE40 at 312°C, and JE50 at 278°C. The higher Tonset for JE40 relative to JE30 and JE50 is noteworthy. At JE40, the intimate fiber–matrix contact – evidenced by SEM – creates a constrained interphase zone where chain mobility is restricted by physical adsorption of epoxy chains onto the cellulose surface, effectively raising the local thermal stability. Conversely, at JE50, the prevalence of poorly consolidated regions and fiber–fiber contacts reduces the effective interfacial area available for this constraint effect and introduces moisture-accessible capillary pathways that may facilitate hydrolytic degradation during thermal ramp [30]. Residual char yields increased monotonically with fiber content (NE: 8.2%, JE30: 14.6%, JE40: 19.3%, JE50: 23.8%), reflecting the higher inherent char-forming tendency of cellulosic matter.

DSC thermograms (Figure 8) from the second heating scan revealed glass transition temperatures (Tg) of 94°C (NE), 96°C (JE30), 98°C (JE40), and 95°C (JE50). The marginal increase in Tg with fiber addition (particularly for JE40) is consistent with restricted chain segmental mobility imposed by the fiber–matrix interfacial region – an effect described in the literature as the "interphase confinement" mechanism [31]. The small magnitudes of Tg variation (within 4°C across all compositions) suggest that the fiber reinforcement does not substantially perturb the bulk epoxy network cross-link density, which is primarily governed by the resin/hardener stoichiometry maintained constant across all formulations in Table 5.

**Table 5.** Thermal characterization parameters from TGA and DSC analysis.

| Sample | Tonset (°C) | Tpeak (°C) | Residual weight at 700°C (%) | Tg from DSC (°C) |
|---|---|---|---|---|
| Neat Epoxy (NE) | 348 ± 3 | 392 ± 4 | 8.2 ± 0.5 | 94 ± 1 |
| JE30 | 284 ± 4 | 341 ± 5 | 14.6 ± 0.8 | 96 ± 1 |
| JE40 | 312 ± 3 | 367 ± 4 | 19.3 ± 0.9 | 98 ± 1 |
| JE50 | 278 ± 5 | 328 ± 6 | 23.8 ± 1.1 | 95 ± 2 |

 

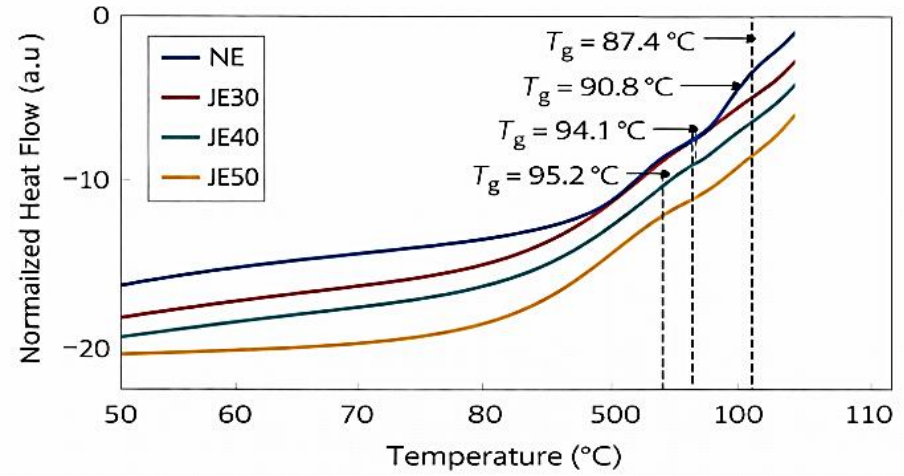


**Figure 8.** DSC thermograms (second heating scan) of NE, JE30, JE40, and JE50.

**Morphological Discussion**

SEM micrographs of tensile fracture surfaces provided direct morphological evidence correlating with the mechanical and thermal property trends. Neat epoxy (Figure 3(a)) exhibited a characteristic featureless, brittle river-mark fracture pattern with smooth crack propagation planes, indicative of limited energy dissipation – consistent with its low impact resistance (9.9 kJ/m²).

JE30 fracture surfaces (Figure 3(b)) showed partially pulled-out fibers leaving cylindrical voids in the matrix, alongside matrix microcracks propagating perpendicular to the fiber axis. The relatively long fiber pull-out lengths (~0.8–1.2 mm) suggest incomplete interfacial bonding even after alkali treatment, likely due to insufficient fiber–matrix contact area at this lower fiber fraction allowing crack deflection along fiber–matrix interfaces rather than through the fiber cross-section [32].

JE40 exhibited the most favorable fracture morphology (Figure 3(c)): short fiber pull-out lengths (<0.3 mm), evidence of matrix shear banding adjacent to fiber–matrix interfaces, and occasional fiber fracture (rather than debonding), all indicative of strong interfacial adhesion capable of transferring stresses sufficient to exceed the fiber tensile strength. This observation directly supports the peak mechanical performance recorded for JE40 across tensile, flexural, and impact modes. The higher Tonset (312°C) of JE40 relative to adjacent compositions is further consistent with this intimate interfacial contact restricting the diffusion of degradation products.

JE50 fracture surfaces (Figure 3(d)) displayed extensive fiber bundling, matrix-starved regions visible as irregular resin-free channels between fiber bundles, and large fiber pull-out zones exceeding 1.5 mm. These features directly explain the property reduction at Vf = 50%: stress concentrations at void-fiber bundle interfaces initiate premature failure, and the reduced effective matrix volume diminishes energy absorption capacity in both mechanical and thermal regimes [33].

**STRUCTURAL APPLICATION ASSESSMENT**

The structural utility of a composite material is often evaluated through its specific properties – mechanical performance normalized by density – which governs lightweight application feasibility. The JE40 composite exhibits a measured density of 1.31 g/cm³ (calculated from Equation 4), representing a 6.5% reduction relative to conventional E-glass/epoxy composite (~1.85 g/cm³):

$$\rho c = \rho f \cdot Vf + \rho m \cdot Vm \quad (4)$$

The specific tensile strength of JE40 (87.4 MPa / 1.31 g/cm³ = 66.7 MPa·cm³/g) compares favorably against reported values for E-glass/epoxy (~68–72 MPa·cm³/g at similar volume fractions), despite the

 

absolute tensile strength of the jute composite being approximately 40% lower in Table 6. This near-equivalent specific performance, combined with the substantially lower environmental burden of jute cultivation, positions alkali-treated jute/epoxy composites as viable replacements for GFRPs in non-primary structural applications including automotive interior panels, transit bus body components, construction formwork, sports equipment housings, and agricultural machinery shrouding [34].

Table 6 provides a systematic comparison of JE40 mechanical properties against E-glass/epoxy and selected literature NFCs, confirming that JE40 achieves competitive specific properties, particularly in flexural stiffness and impact energy, while offering significant advantages in density, biodegradability, and estimated embodied energy (~18 MJ/kg for jute fiber vs. ~54 MJ/kg for E-glass fiber) [35].

**Table 6.** Comparative mechanical properties of JE40 composite against E-glass/epoxy and representative natural fiber composites from literature.

| Property | JE40 (this study) | E-glass/epoxy [Ref. 32] | Hemp/epoxy [Ref. 33] | Sisal/epoxy [Ref. 26] |
|---|---|---|---|---|
| Vf (%) | 40 | 40 | 40 | 40 |
| Density (g/cm³) | 1.31 | 1.85 | 1.28 | 1.34 |
| Tensile Strength (MPa) | 87.4 | 220.4 | 68.2 | 79.6 |
| Flexural Strength (MPa) | 112.6 | 145.2 | 86.3 | 107.4 |
| Impact Energy (kJ/m²) | 18.7 | 24.3 | 14.2 | 16.8 |
| Specific Tensile Strength (MPa·cm³/g) | 66.7 | 119.1 | 53.3 | 59.4 |
| Embodied Energy (MJ/kg fiber) | ~18 | ~54 | ~15 | ~14 |
| Biodegradable | Yes | No | Yes | Yes |

## CONCLUSION

This study systematically investigated the mechanical and thermal performance of alkali-treated jute fiber reinforced epoxy composites fabricated via a combined hand lay-up and compression molding process at fiber volume fractions of 30%, 40%, and 50%. The results demonstrate that fiber incorporation significantly enhances stiffness, strength, and impact resistance relative to neat epoxy, provided that fiber loading remains within an optimal range. Among the investigated formulations, the JE40 composite exhibited the most balanced performance profile, achieving peak tensile and flexural strengths along with maximum Charpy impact energy. The superior behavior at 40 vol% is attributed to improved fiber–matrix interfacial adhesion following NaOH treatment, effective stress transfer, and minimized void content.

At higher fiber loading (50 vol%), mechanical properties declined despite increased reinforcement content. This reduction is associated with fiber agglomeration, matrix-starved regions, and increased void fraction, all which compromise load transfer efficiency and promote premature crack initiation. Thermal analysis further confirmed that composite performance is strongly governed by interfacial interactions. JE40 exhibited enhanced onset degradation temperature relative to adjacent formulations, while DSC results revealed a modest increase in glass transition temperature with fiber addition, reflecting interfacial chain confinement effects without significant alteration of bulk crosslink density.

From a structural application standpoint, the optimized jute/epoxy system demonstrates competitive specific mechanical properties when benchmarked against conventional glass fiber composites, while offering substantial advantages in density reduction, biodegradability, and embodied energy. These findings support the feasibility of alkali-treated jute fiber composites for lightweight semi-structural components in automotive interiors, construction panels, and consumer product housings where sustainability and weight efficiency are critical design drivers.

### Future Scope

While the present investigation establishes the optimal fiber loading and confirms the effectiveness of alkali treatment in enhancing interfacial bonding, several avenues remain open for further

 

advancement. The incorporation of hybrid reinforcement architecture – such as outer glass fiber plies combined with jute core layers or intra-ply natural fiber hybridization – may enable further improvements in strength while preserving sustainability advantages.

The integration of nano-scale fillers within the epoxy matrix represents another promising pathway to enhance matrix-dominated properties including interlaminar shear strength, fracture toughness, and thermal stability. Cellulose nanocrystals, nano-clay, or graphene derivatives could synergistically interact with treated fiber surfaces to reinforce the interphase region.

Long-term durability under environmental exposure also warrants systematic investigation. Hygrothermal aging, moisture diffusion modeling, and mechanical retention studies are essential for realistic structural qualification, given the inherent hydrophilicity of lignocellulosic fibers. Fatigue performance under cyclic loading conditions should likewise be evaluated to establish service life predictions for structural deployment.

Finally, advanced surface modification strategies – such as silane coupling, plasma treatment, or dual-stage chemical functionalization, should be comparatively assessed against the NaOH baseline to optimize interfacial chemistry and further elevate composite reliability under mechanical and thermal stress.

## REFERENCES

1. Sanjay MR, Siengchin S, Parameswaranpillai J, Jawaid M, Pruncu CI, Khan A. A comprehensive review of techniques for natural fibers as reinforcement in composites: Preparation, processing and characterization. Carbohydr Polym. 2019;207:108–121.
2. Mohammed L, Ansari MNM, Pua G, Jawaid M, Islam MS. A review on natural fiber reinforced polymer composite and its applications. Int J Polym Sci. 2015;2015:1–15.
3. Pickering KL, Aruan Efendy MG, Le TM. A review of recent developments in natural fibre composites and their mechanical performance. Compos Part A Appl Sci Manuf. 2016;83:98–112.
4. Ramakrishnan S, Krishnamurthy K, Rajasekar R, Rajeshkumar G. Effect of nano-silica addition on the static and dynamic mechanical properties and structural integrity of kenaf/carbon fiber reinforced epoxy based composites for structural applications. J Inorg Organomet Polym Mater. 2021;31(3):1021–1034.
5. La Rosa AD, Recca G, Summerscales J, Latteri A, Cozzo G, Cicala G. Bio-based versus traditional polymer composites. A life cycle assessment perspective. J Clean Prod. 2014;74:135–144.
6. Pico D, Steinmann W. Synthetic fibers and textiles: Fundamentals of production and properties. In: Matteson NJ, editor. Fibers. Cham: Springer; 2016. p. 48–95.
7. Witik RA, Teuscher R, Michaud V, Ludwig C, Månson JAE. Carbon fibre reinforced polymer composites: The environmental benefit of fibre recycling. Resour Conserv Recycl. 2013;70:16–26.
8. Duflou JR, Deng Y, Van Acker K, Dewulf W. Do fiber-reinforced polymer composites provide environmentally benign alternatives? A life-cycle-assessment-based study. MRS Bull. 2012; 37(4):374–382.
9. Faruk O, Bledzki AK, Fink HP, Sain M. Biocomposites reinforced with natural fibers: 2000–2010. Prog Polym Sci. 2012;37(11):1552–1596.
10. Omrani E, Menezes PL, Rohatgi PK. State of the art on tribological behavior of polymer matrix composites reinforced with natural fibers in the green materials world. Eng Sci Technol. 2016;19(2):717–736.
11. Jawaid M, Khalil HPSA. Cellulosic/synthetic fibre reinforced polymer hybrid composites: A review. Carbohydr Polym. 2011;86(1):1–18.
12. Salit MS. Tropical natural fibre composites: Properties, manufacture and applications. Singapore: Springer; 2014.
13. Li X, Tabil LG, Panigrahi S. Chemical treatments of natural fiber for use in natural fiber-reinforced composites: A review. J Polym Environ. 2007;15(1):25–33.

 

14. Oushabi A, Sair S, Hassani FO, Abboud Y, Tanane O, El Bouari A. The effect of alkali treatment on mechanical, morphological and thermal properties of date palm fibers (DPFs): Study of the interface of DPF–polyurethane composite. S Afr J Chem Eng. 2017;23:116–123.
15. Kabir MM, Wang H, Lau KT, Cardona F. Chemical treatments on plant-based natural fibre reinforced polymer composites: An overview. Compos Part B Eng. 2012;43(7):2883–2892.
16. Roy A, Chakraborty S, Kundu SP, Basak RK, Majumder SB, Adhikari B. Improvement in mechanical properties of jute fibres through mild alkali treatment as assessed by utilisation of the Weibull distribution model. Bioresour Technol. 2012;107:222–228.
17. Nair LS, Laurencin CT. Biodegradable polymers as biomaterials. Prog Polym Sci. 2007;32(8–9):762–798.
18. Mochane MJ, Mokhena TC, Mokhothu TH, Mtibe A, Sadiku ER, Ray SS, et al. Recent progress on natural fiber hybrid composites for advanced applications: A review. eXPRESS Polym Lett. 2019;13(2):159–198.
19. Siakeng R, Jawaid M, Ariffin H, Sapuan SM, Asim M, Saba N. Natural fiber reinforced polylactic acid composites: A review. Polym Compos. 2019;40(2):446–463.
20. Godase V, Khiste R, Palimkar V. AI-optimized reconfigurable antennas for 6G communication systems. J RF Microw Commun Technol. 2025;2(3):1–12. Bhaganagare S, Chavan S, Gavali S, Godase VV. Voice-controlled home automation with ESP32: A systematic review of IoT-based solutions. J Microprocess Microcontrol Res. 2025;2(3):1–13.
21. Rajak DK, Pagar DD, Menezes PL, Linul E. Fiber-reinforced polymer composites: Manufacturing, properties, and applications. Polymers. 2019;11(10):1667.
22. Vinod A, Sanjay MR, Suchart S, Jyotishkumar P. Renewable and sustainable biobased materials: An assessment on biofibre reinforced polymer composites. J Clean Prod. 2020;258:120978.
23. Jamadade VK, Ghodke MG, Katakdhond SS, Godase V. A review on real-time substation feeder power line monitoring and auditing systems. Int J Emerg IoT Technol Smart Electron Commun. 2025;1(2):1–16.
24. Jagadeesh D, Sudhakara P, Lee JS, Kim BS. Multi-objective optimization of mechanical properties on bagasse fiber/polyester composites using grey relational analysis. Mater Today Commun. 2021;26:102161.
25. Godase V. Graphene-based nano-antennas for terahertz communication. Int J Digit Electron Microprocess Technol. 2025;1(2):1–14.
26. Sathishkumar TP, Naveen J, Satheeshkumar S. Hybrid fiber reinforced polymer composites – A review. J Reinf Plast Compos. 2014;33(5):454–471.
27. Fragassa C, Pavlovic A, Santulli C. Mechanical and impact characterisation of flax and basalt fibre bio-vinylester composites and their hybrids. Compos Part B Eng. 2018;137:247–259.
28. Ramesh M, Deepa C, Tamil Selvan M, Rajeshkumar L, Balaji D, Bhuvaneswari V. Influence of fiber surface treatment on the mechanical and tribological properties of Calotropis gigantea plant fiber reinforced polymer composites. Polym Compos. 2021;42(9):4308–4320.
29. Yang H, Yan R, Chen H, Lee DH, Zheng C. Characteristics of hemicellulose, cellulose and lignin pyrolysis. Fuel. 2007;86(12–13):1781–1788.
30. Dhakal HN, Zhang ZY, Richardson MOW. Effect of water absorption on the mechanical properties of hemp fibre reinforced unsaturated polyester composites. Compos Sci Technol. 2007;67(7–8):1674–1683.
31. Saba N, Jawaid M, Alothman OY, Paridah MT. A review on dynamic mechanical properties of natural fibre reinforced polymer composites. Constr Build Mater. 2016;106:149–159.
32. Ku H, Wang H, Pattarachaiyakoop N, Trada M. A review on the tensile properties of natural fiber reinforced polymer composites. Compos Part B Eng. 2011;42(4):856–873.
33. Shahzad A. Hemp fiber and its composites – A review. J Compos Mater. 2012;46(8):973–986.
34. Thyavihalli Girijappa YG, Mavinkere Rangappa S, Parameswaranpillai J, Siengchin S. Natural fibers as sustainable and renewable resource for development of eco-friendly composites: A comprehensive review. Front Mater. 2019;6:226.
35. Moudood A, Rahman A, Öchsner A, Islam M, Francucci G. Flax fiber and its composites: An overview of water and moisture absorption impact on their performance. J Reinf Plast Compos. 2019;38(7):323–339.

 